Manipulating surface plasmon waves by transformation optics: Design examples of a beam squeezer, bend, and omnidirectional absorber*

Yu Zhen-Zhong(余振中), Feng Yi-Jun(冯一军)†, Wang Zheng-Bin(王正斌), Zhao Jun-Ming(赵俊明), and Jiang Tian(姜 田)

Department of Electronic Engineering, School of Electronic Science and Engineering, Nanjing University, Nanjing 210093, *China*

(Received 7 July 2012; revised manuscript received 3 September 2012)

We present several design examples of how to apply transformation optics and curved space under coordinate transformation to manipulating the surface plasmon waves in a controlled manner. We demonstrate in detail the design procedure of the plasmonic wave squeezer, in-plane bend and omnidirectional absorber. We show that the approximation method of modifying only the dielectric material of a dielectric–metal surface of the plasmonic device could lead to acceptable performance, which facilitates the fabrication of the device. The functionality of the proposed plasmonic device is verified using three-dimensional full-wave electromagnetic simulations. Aiming at practical realization, we also show the design of a plasmonic in-plane bend and omnidirectional absorber by an alternative transformation scheme, which results in a simple device structure with a tapered isotropic dielectric cladding layer on the top of the metal surface that can be fabricated with existing nanotechnology.

Keywords: transformation optics, surface plasmon polaritons, metamaterial

PACS: 41.20.Jb, 73.20.Mf, 78.67.Pt **DOI:** 10.1088/1674-1056/22/3/034102

1. Introduction

In recent years, much attention has been given to transformation optics (TO) which have the potential ability to arbitrarily manipulate electromagnetic (EM) wave propagation. The TO method is based on the form-invariant of Maxwell's equations under different coordinate transformations,[1,2] and can be used to design novel devices that control the EM waves with the pre-defined distribution of material constitutive parameters implemented through artificial metamaterials.[1,2] The most important example that has been proposed and designed by means of TO, are the invisibility cloaks that can guide light around the desired hidden region, making it transparent to external observation.[1–5] Various other unprecedented devices have also been proposed, such as the EM field concentrator,[6] beam bend,[7,8] beam splitter,[8,9] beam squeezer[10,11] and omnidirectional absorber.[12–15]

Surface plasmon polaritons (SPPs) are surface electromagnetic waves propagating along the dielectric–metal interface.[16,17] These surface waves are well confined along the interface, and become evanescent in the direction perpendicular to the interface with their field magnitude exponentially decaying both in the metal and on the dielectric sides. As the surface waves are limited to sub-wavelength scales, this could lead to miniaturized optical integrated circuits and devices with scales smaller than the light wavelength.[18,19]

As TO is based on the form-invariant of Maxwell's equations, it may be applied to all EM waves including SPPs. Recently, some effort has been made in the successful application of TO to the efficient manipulation of SPP waves.[20–25] With the help of metamaterials, different plasmonic structures have been theoretically proposed to manipulate SPP waves, such as the invisibility cylinder or carpet cloak, SPP beam shifter, concentrator, and rotator.[20–24] Besides the theoretical studies, experimental explorations have been carried out on constructing and verifying the performances of a plasmonic Luneburg lens and a plasmonic Eaton lens by spatially varying the thickness of a thin dielectric film on the metal.[25]

In this paper, we continue the theoretical studies on designing plasmonic structures and devices for manipulating the SPPs through TO. We present three examples: an SPP beam squeezer, a bend and an omnidirectional concentrator. Detailed design procedures and three-dimensional (3D) full-wave simulations will be demonstrated to verify their functionality. Firstly, we present a beam squeezer for SPPs with anisotropic and inhomogeneous transformed materials. Secondly, we numerically demonstrate an in-plane wave bend based on both transformation optics and geometrical optics. Focused on practical applications, we finally focus on the design of the SPP wave bend and omnidirectional absorber constructed by conventional dielectric cladding with varying thicknesses on a silver surface, which could facilitate the practical realization.

*Project supported by the National Natural Science Foundation of China (Grant Nos. 60990322, 60990320, 60801001, and 61101011) and the Specialized Research Fund for Doctoral Program of Higher Education of China (Grant No. 20100091110036).

†Corresponding author. E-mail: yjfeng@nju.edu.cn

© 2013 Chinese Physical Society and IOP Publishing Ltd

2. SPP devices designed by transformation optics

The TO is based on the form-invariance of Maxwell's equations under coordinate transformation. It provides a useful way to arbitrarily manipulate the EM waves through metamaterials whose constitutive parameters can be determined through particularly chosen coordinate transformation. By mapping an area in the free space with a distorted coordinate (virtual) to a medium with constitutive tensors ε and μ in a physical space with a uniform coordinate, we are able to route the EM propagation characterized by the distorted coordinate. The mathematical formalism used for the calculation of the permittivity and permeability tensors of the functional material can be summarized as follows. For a spatial coordinate transformation between the virtual space (x', y', z') and the transformed physical space (x, y, z), the coordinate transformation can be described by the Jacobian matrix $\boldsymbol{J}$ as

$$\boldsymbol{J} = \begin{pmatrix} \frac{\partial x}{\partial x'} & \frac{\partial x}{\partial y'} & \frac{\partial x}{\partial z'} \\ \frac{\partial y}{\partial x'} & \frac{\partial y}{\partial y'} & \frac{\partial y}{\partial z'} \\ \frac{\partial z}{\partial x'} & \frac{\partial z}{\partial y'} & \frac{\partial z}{\partial z'} \end{pmatrix}. \tag{1}$$

Enforcing the form-invariance of Maxwell's equations in either coordinate, the material tensors ε and μ for the medium in the physical space can be determined by

$$\varepsilon = \frac{\boldsymbol{J}\varepsilon_0\boldsymbol{J}^{\mathrm{T}}}{\det(\boldsymbol{J})}, \quad \mu = \frac{\boldsymbol{J}\mu_0\boldsymbol{J}^{\mathrm{T}}}{\det(\boldsymbol{J})}, \tag{2}$$

where ε_0 and μ_0 are the permittivity and permeability of the free space.

As TO is applied to all EM waves, it can be extended to SPPs. A rigorous TO process applied to SPP structures should require coordinate transformation on both the dielectric and the metal sides of the interface. However, it has been shown that modifying only the EM propagation on the dielectric side is also feasible and results in relatively simple structures due to much smaller decay length of SPP waves in the metal.[21,22]

2.1. SPP beam squeezer

For the first example, we consider a plasmonic beam squeezer that can be used for modulating the SPP beam width as sketched in Fig. 1(b). We begin with a two-dimensional (2D) squeezer structure designed by an exponential coordinate

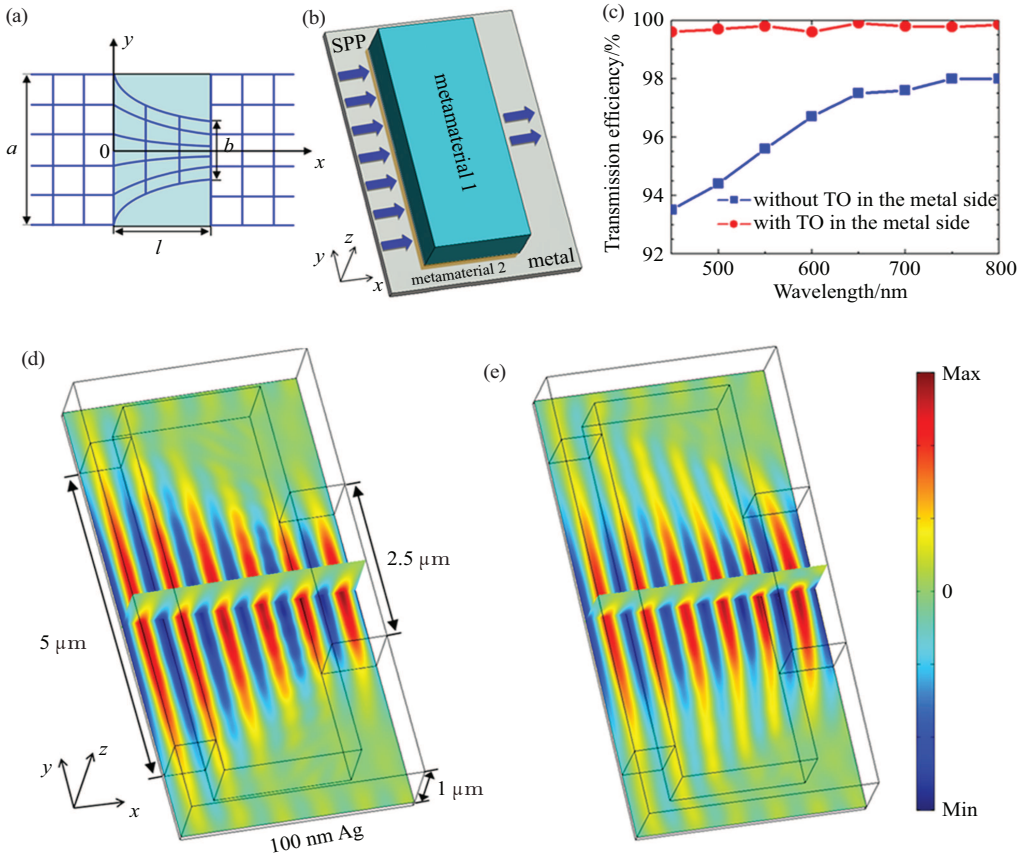


Fig. 1. (color online) (a) The transformed space for designing a two-dimensional squeezer with an exponential transformation. (b) A three-dimensional schematic picture for a plasmonic squeezer. (c) Transmission efficiencies of the plasmonic squeezer in an optical range. Blue squares: without TO on the metal side; red circles: with TO on the metal side. (d) The electric field E_z distribution at 600 nm wavelength for a plasmonic squeezer with transformed materials on both the dielectric and metal sides (e) The electric field E_z distribution when a transformation material is inserted only on the dielectric side.

transformation similar to that discussed in Ref. [11]. This exponential transformation maps a 2D rectangular region sized by l and a into a taper with the output width b, shown in Fig. 1(a). The exponential transformation formula is written as

$$x = x', \quad y = y'(b/a)^{x'/l}, \quad z = z'. \tag{3}$$

According to the TO, the material parameters of this slab in the Cartesian coordinates (x, y, z) can be expressed through Eq. (2) as

$$\varepsilon/\varepsilon_0 = \mu/\mu_0 = \begin{pmatrix} \varepsilon_{xx} & \varepsilon_{xy} & 0 \\ \varepsilon_{xy} & \varepsilon_{yy} & 0 \\ 0 & 0 & \varepsilon_{zz} \end{pmatrix}, \tag{4}$$

where $\varepsilon_{xx} = \varepsilon_{zz} = (b/a)^{-x/l}$, $\varepsilon_{xy} = \varepsilon_{xx} y \ln(b/a)/l$, and $\varepsilon_{yy} = 1/\varepsilon_{xx} + \varepsilon_{xy}^2/\varepsilon_{xx}$.

Other coordinate transformations can be used to generate a beam squeezer, but compared with that from linear and parabolic transformations,[11] the material parameters deduced from exponential transformation exhibit slow variation in spatial distribution.

Next, we extend the above-mentioned 2D transformation results to a 3D beam squeezer for SPPs propagating along the interface (at $z = 0$) of two semi-infinite regions, which are filled with dielectric (upper region) and silver (lower region), respectively. The relative permittivity of silver is given by the Drude model as follows:

$$\varepsilon_{\mathrm{m}}(\omega) = \varepsilon_\infty - \frac{\omega_{\mathrm{p}}^2}{\omega(\omega + \mathrm{i}\gamma_{\mathrm{c}})}, \tag{5}$$

where ε_∞ is a constant that describes the contribution from interband transitions at infinite frequency, ω_{p} is the plasma frequency, and γ_{c} is the damping rate ($\varepsilon_\infty = 3.7$, $\omega_{\mathrm{p}} = 9.1$ eV, $\gamma = 0.018$ eV).[26] In rigorous TO framework, in order to control the SPPs in designed manner, we should manipulate the transformation of material parameters on both the dielectric and the metal sides, with metamaterials 1 and 2 as shown in Fig. 1(b). On the dielectric side, the material parameters are expressed in Eq. (4). On the metal side, the material tensors are transformed to

$$\varepsilon_{\mathrm{m}} = \varepsilon_{\mathrm{m}}\varepsilon, \quad \mu_{\mathrm{m}} = \mu_{\mathrm{m}}\mu, \tag{6}$$

where the relative permeability of silver $\mu_{\mathrm{m}} = 1$. To confirm the performance of the SPP beam squeezer, full-wave EM simulation is carried out using the commercial COMSOL MULTIPHYSICS package. A Gaussian SPP wave propagating along the air-silver interface at wavelength $\lambda = 600$ nm is perpendicularly incident on the transformed slab composed of metamaterials 1 and 2 designed with $a = 6$ μm, $l = 2$ μm and $b = 3$ μm. Therefore, when we set the incident Gaussian SPP with width 5 μm, the width of the output should be squeezed to 2.5 μm in theory, which is verified well in Fig. 1(d). To study the broadband functionality of this device, the power flow transmission efficiencies of SPPs through the beam squeezer are calculated at different optical wavelengths, which are shown in Fig. 1(c). The transmission efficiency is defined as the ratio of power flow between the output and the input ports. In the process of simulation, we have neglected the loss of the silver so as to only investigate the effectiveness of the transformed medium, and the incident Gauss SPP waves at different wavelengths are set to have the same beam width. When a rigorous TO is used, both the dielectric and the metal materials are transformed. Thus, the transmission efficiency of SPPs is almost 100% over the wavelength range.

We also compare the results with those of the approximate case that only the dielectric side (upper region) is transformed under TO. Without the transformation on the metal side, the transmission efficiency of the beam squeezer decreases slightly from a value of 98% at 800 nm to 93.5% at 450 nm. There are two reasons for this slight degradation. On the one hand, as most energy of the surface wave is confined on the dielectric side, the transformation only for the dielectric side cannot obviously affect the desired performance.[21–23] On the other hand, the SPP energy on the metal side increases with frequency, which leads to the increased reduction of the transmission at short wavelengths. Figures 1(d) and 1(e) show the electric field distributions with and without the transformation on the metal side, respectively. It is worth mentioning that there is no significant difference in field distribution between the two cases as shown in Figs. 1(d) and 1(e).

2.2. SPP wave in-plane bend

Manipulating the surface plasmonic wave along a bended dielectric–metal interface has been recently studied in a 2D case under the framework of geometric optics.[22] Here, as a second example, we discuss the beam bend within the plane dielectric–metal interface for SPPs which is capable of changing the direction of the surface waves in a 3D case. Such an in-plane beam bend can be achieved by using either the TO or geometrical optics.[7,8] As regards to the TO, a 2D bend is obtained from a Cartesian-to-polar coordinate transformation, where a $b \times b$ square area in a Cartesian coordinate is transformed into fan-shaped region in a polar coordinate.[8] Figure 2(a) shows the fan-shaped region in the transformed coordinate system with the inner radius $r = a$ and outer radius $r = b$. The relative material constitutive parameters of the beam bend can be expressed in the cylindrical (r, φ, z) coordinate as

$$\varepsilon/\varepsilon_0 = \mu/\mu_0 = \begin{bmatrix} 2b/\pi r & 0 & 0 \\ 0 & \pi r/2b & 0 \\ 0 & 0 & 2b/\pi r \end{bmatrix}. \tag{7}$$

By applying this material transformation to both the dielectric and metal sides of a dielectric–metal interface, we can realize a beam bend for SPPs with metamaterials 1 and 2 as shown in Fig. 2(b). The material parameters of metamaterials 1 and 2 are obtained by

$$\begin{cases} \varepsilon_{\rm d} = \varepsilon, \quad \mu_{\rm d} = \mu, \\ \varepsilon_{\rm m} = \varepsilon_{\rm m}\varepsilon, \quad \mu_{\rm m} = \mu_{\rm m}\mu, \end{cases} \tag{8}$$

where $\varepsilon_{\rm m}$ and $\mu_{\rm m}$ are the relative permittivity and permeability of metal chosen here as silver. The performances of a right-angle SPP bend were verified with COMSOL simulation at wavelength $\lambda = 600$ nm. The SPP beam with Gaussian magnitude distribution in the y direction propagates perpendicularly into one side of the bend as shown in Fig. 2(b). The dimensions of the bend are $a = 0.55$ μm and $b = 4.4$ μm, and the central axis of the incident SPPs is at $y = 2.1$ μm. Figure 2(c) shows the 3D simulation of the right-angle bend for SPPs when the transformation is applied to both the dielectric and metal side. In such an ideal case, the output direction of SPP propagation from the bend is rotated by 90° from the $+x$ direction to the $-y$ direction. We also compare the case when transformation is only applied to the dielectric side. The resulting field distribution is displayed in Fig. 2(d). It shows that the propagation trajectory of SPPs has little difference between the two cases.

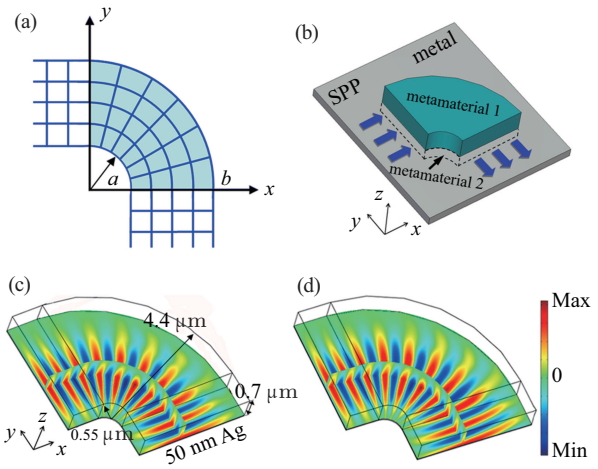


Fig. 2. (color online) (a) The transformed space for designing a two-dimensional bend. (b) A three-dimensional schematic picture for a beam bend for SPPs. (c) The electric field E_z distribution of SPPs at 600 nm wavelength for a three-dimensional beam bend based on the transformation optics. The transformed materials are both on the dielectric and metal side. (d) The bend when the transformed material is only used on the dielectric side.

Another way to design a bend for SPPs is based on geometrical optics.[7] The design requires only isotropic material, and is easy for practical implementation in comparison with the method based on the TO. The material parameters of the nonmagnetic bend on the dielectric side can be expressed as

$$\varepsilon = \varepsilon_0(A/r)^2, \quad \mu = \mu_0, \tag{9}$$

where A is a constant. In order to allow the SPPs to propagate synchronously on both the dielectric and the metal side, the material parameters on the metal side should satisfy

$$\varepsilon_{\rm m} = \varepsilon_{\rm m}\varepsilon_0(A/r)^2, \quad \mu_{\rm m} = \mu_0. \tag{10}$$

Figure 3(a) shows the ideal performance of the 3D beam bend of SPPs at 600 nm wavelength, when the material parameters on the dielectric and metal side are obtained under geometrical optics from Eqs. (9) and (10), respectively. Figure 3(b) illustrates the corresponding performance of an SPP bend in which only the dielectric side is filled with the designed material from Eq. (9). In this case, the deflection angle of the SPP beam is slight larger than 90°, which may be caused by the unbalanced material parameters on both sides of the dielectric–metal interface for the SPPs. Therefore, it is necessary to revise the material parameter distribution on the dielectric side when the metal side is kept unchanged. When adopting the modified permittivity as $\varepsilon = \varepsilon_0(A/r)^{1.8}$ on the dielectric side, we could achieve a similar performance to that in the ideal case, which is shown in Fig. 3(c).

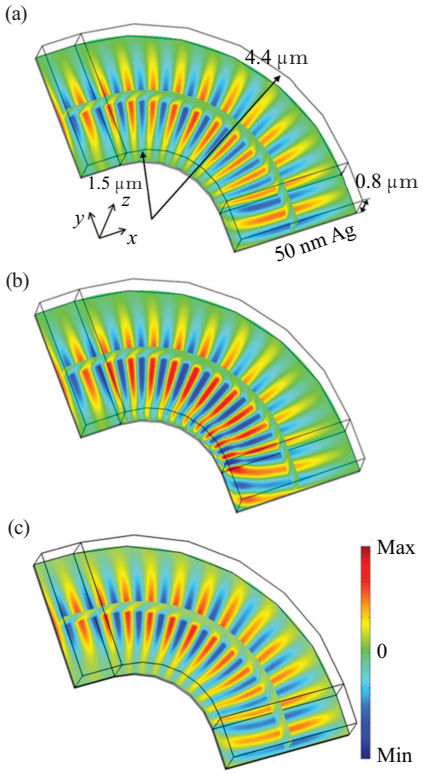


Fig. 3. (color online) (a) The electric field E_z distribution of SPPs at 600 nm wavelength for a three-dimensional beam bend. The material parameters on the dielectric and metal side are obtained from geometrical optics (b) The bend for SPPs when the material is only on the dielectric side is obtained by geometrical optics. (c) The bend with revised refractive index on the dielectric side.

3. Realization examples with realistic materials

The SPP devices designed under the TO framework sometimes cause their materials to be anisotropic, i.e., inhomogeneous permittivity and permeability tensors, thus they

are difficult to realize. However, by adopting appropriate transformation, isotropic material parameter may be obtained, which facilitates the implementation of the device. For example, the plasmonic device with horizontally distributed isotropic material on the dielectric side can be accomplished by a dielectric layer with varying thickness cladding on the metal.[22,25] Modulating the thickness of the middle dielectric in the dielectric/dielectric/metal (DDM) hetero-structure, we can change the effective mode index of SPPs. The implicit expression of the dispersion relationship for this hetero-structure can be described as[17]

$$e^{-2k_1 d} = \frac{k_1/\varepsilon_1 + k_2/\varepsilon_2}{k_1/\varepsilon_1 - k_2/\varepsilon_2} \frac{k_1/\varepsilon_1 + k_m/\varepsilon_m}{k_1/\varepsilon_1 - k_m/\varepsilon_m}, \tag{11}$$

where the subscripts 1, 2, or m correspond to the middle, top dielectric layer, or the metal substrate, the k is the wave vector perpendicular to the interface in the three media in the hetero-structure, and d is the thickness of the middle dielectric. All the permittivities in Eq. (11) indicate the relative permittivities. The metal permittivity ε_m is determined by the Drude model, and the top dielectric is assumed to be air with $\varepsilon_2 = 1$.

3.1. SPP in-plane bend with isotropic and homogenous materials

In Section 2.2, the SPP in-plane bend designed with geometric optics transformation results in isotropic material parameters, and can be realized utilizing the DDM hetero-structure. In the bend structure the material parameters change with the radius of the fan-shape region, and therefore can be implemented by a cladding dielectric layer with thickness varying with radius. Considering the practical realization, we use SiO_2 as a cladding material whose permittivity is $\varepsilon_1 = 2.4$ in an optical frequency range. According to Eq. (11), the relationship between the thickness d of SiO_2 layer and the radius r for the bend at wavelength $\lambda = 600$ nm is shown in Fig. 4 (solid line). For simplicity, the relationship is approximated by a linear function (straight dashed line) and the corresponding schematic diagram for a 90° bend is illustrated in the inset of Fig. 4. The SiO_2 cladding is of an incomplete cone structure with a conical base of a 1/4 circle ring. The outer and inner radius of the cladding dielectric are $b = 4$ μm and $a = 2$ μm, respectively. The corresponding height is 160 nm. In the simulation, the loss of the silver is neglected, and the input SPP wave is propagating along the $+x$ direction.

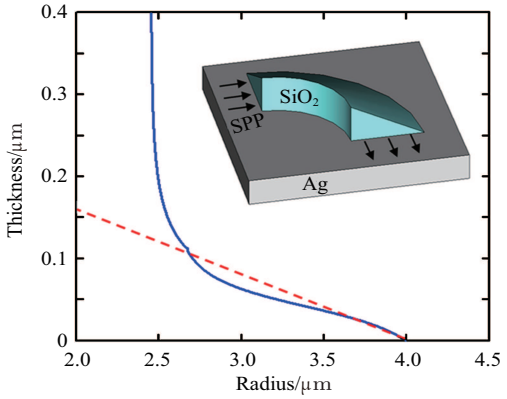


Fig. 4. (color online) The solid line corresponds to the relationship between thickness d of the middle insulator and radius r for the plasmonic bend, and the dashed line is a straight line approximately representing the solid line. The schematic of a bend for SPPs is inserted into the picture.

The 3D simulation of the 90° bend at wavelength $\lambda = 600$ nm is shown in Figs. 5(a) and 5(c). We note that the Gaussian SPPs propagating along the bend undertake a slight compression at the middle position. The transmission efficiency of the SPP bend, determined by the ratio of power flow between the output and the input, is calculated, and the results are shown in Fig. 5(b). The transmission loss is caused mainly by the mismatch at the port boundary, which leads to the parasitic scattering of SPPs into the free-space modes. Connecting two 90° bends, we can obtain a 180° bend for SPPs and the performance is depicted in Fig. 5(d). From the results of the 90° and 180° bends in Fig. 5, these simplified designs for rotating SPPs can achieve good performances.

3.2. SPP omnidirectional absorber by isotropic and homogenous materials

The omnidirectional EM wave absorbers (or sometimes called EM wave black-holes) that can almost completely absorb all incident electromagnetic radiation within a certain radius (radius of the event horizon) have recently been theoretically proposed[12–15] and experimentally realized at microwave frequencies.[14] The absorber proposed by Narimanova and Kildisheva[12] from the approach of Hamiltonian optics is composed of isotropic material, which is different from the anisotropic material required by the Schwarzschild metric in the black hole.[15] Such an omnidirectional absorber designed with isotropic permittivity distribution can be described as follows:[12]

$$\varepsilon(r) = \begin{cases} \varepsilon_0, & r > R, \\ \varepsilon_0 (R/r)^n, & R_c < r < R, \\ \varepsilon_c + i\gamma, & r < R_c, \end{cases} \tag{12}$$

where n is the order number, R is the outer radius of the omnidirectional absorber, and the core radius R_c is regulated by $R_c = R\sqrt[n]{\varepsilon_0/\varepsilon_c}$ to insure the continuity of the real part of the permittivity at the core boundary.

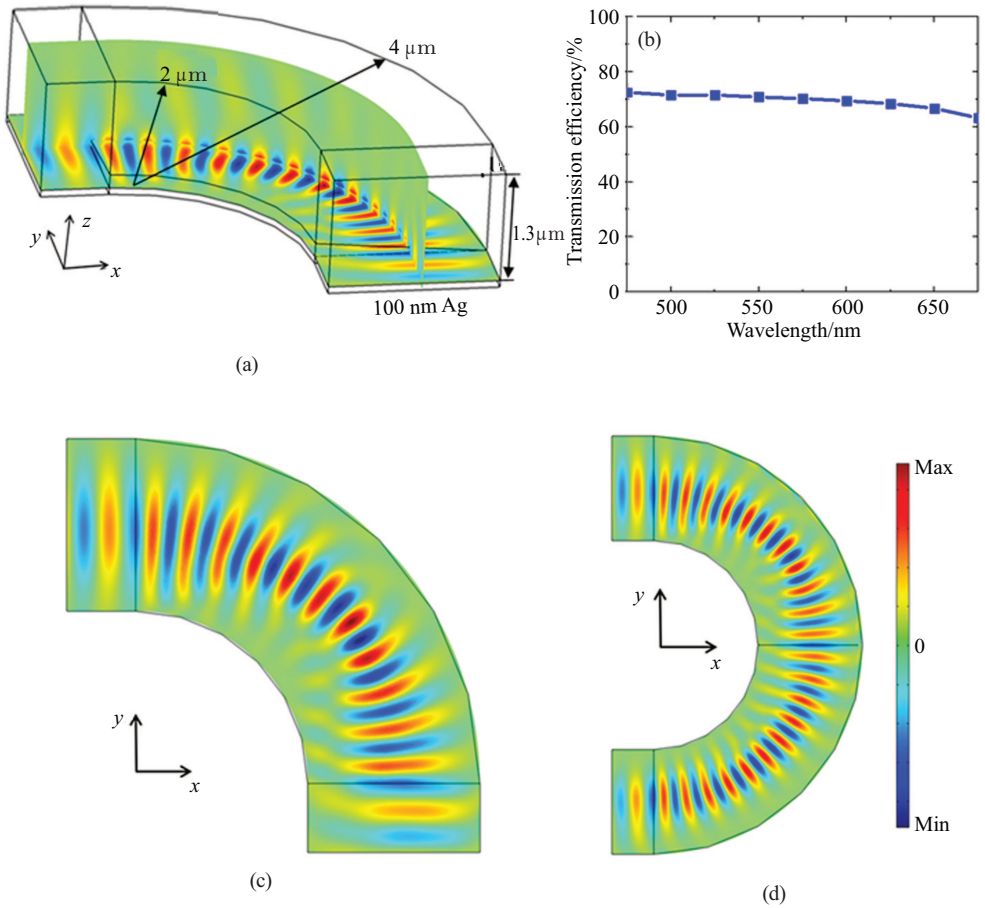


Fig. 5. (color online) (a) The electric field E_z distribution of SPPs at 600 nm wavelength for a 90° bend. (b) Transmission efficiency of the plasmonic 90° bend versus wavelength in optical range. (c) Top view of the electric field for the 90° bend at the metal interface. (d) Top view of the electric field for the 180° bend at the metal interface.

Using the DDM hetero-structure, the SPP omnidirectional absorber can be achieved by an isotropic dielectric layer with varying thickness on the top of the metal surface. Here, we take the design of the omnidirectional absorber as an example, which is composed of an inner dielectric with radius $R_c = 1.9$ μm surrounded by an outer dielectric shell part with tapered thickness and outer radius $R = 3.5$ μm, which is schematically shown in the inset of Fig. 6. The relative permittivities of the cladding dielectric for the outer shell and the inner core are $\varepsilon_1 = 3.5$ and $\varepsilon_c + i\gamma = 3.5 + 0.35i$, respectively. Similarly to the previous example, we calculate the values of thickness d of each cladding layer as a function of position corresponding to the radius r for the omnidirectional absorber with order $n = 2$ and 3, respectively, which are shown in Fig. 6. The curve corresponding to order $n = 2$ has a moderate variation and can be approximated by a linear function as a straight line.

We simulate the SPP wave propagations of a Gaussian beam incident at different positions along the y axis. From Fig. 7, we can observe that the incident SPPs that hit the outer shell are bent to the inner core and the SPP energy is absorbed by the omnidirectional absorber for different incident positions. Due to the circular symmetry associated with the device, it functions to all incident waves that hit the outer shell, thus forming an omnidirectional EM wave absorber.

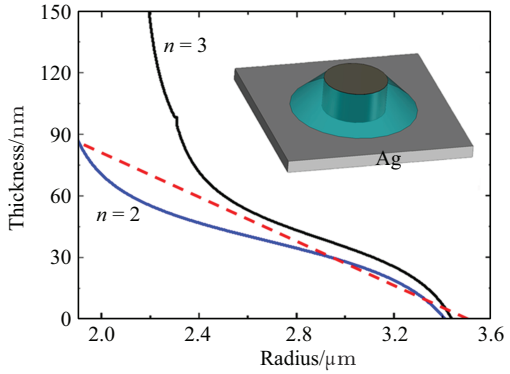


Fig. 6. (color online) The two solid curves correspond to the relationship between the thickness d and radius r for the plasmonic omnidirectional absorber with $n = 2$ and $n = 3$, respectively. The dashed line represents the result for the simplified structure. The inset shows the simplified design for the omnidirectional absorber.

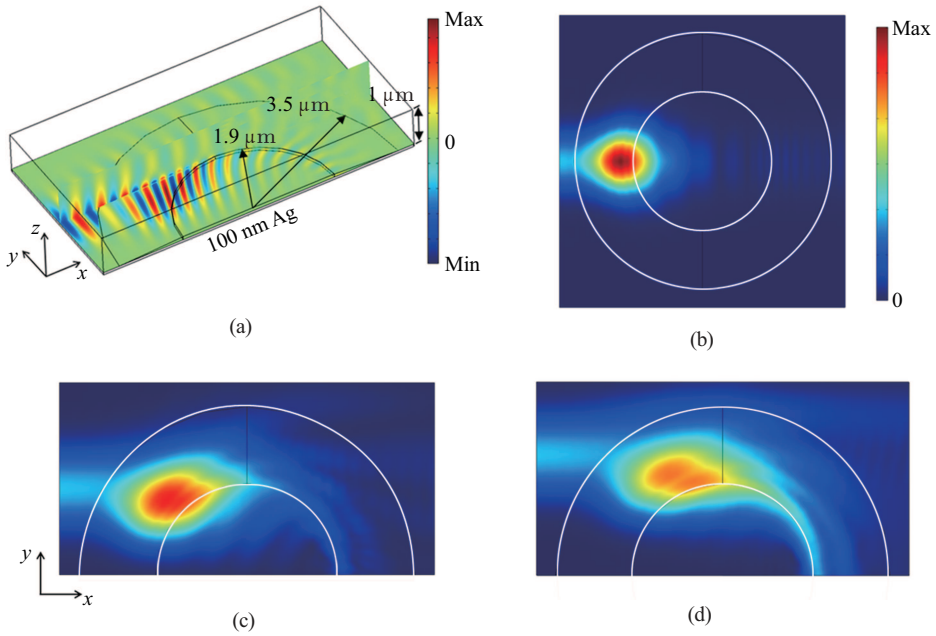


Fig. 7. (color onine) (a) Three-dimensional simulation of electric field E_z distribution for the plasmonic omni-directional absorber at wavelength 632.8 nm. The central position of incident SPPs is 1.8 μm at the y axis. (b) Magnitude of the magnetic field at the metal interface for the central incidence on the inner core. (c) Magnitude of the magnetic field at the metal interface when the central position of incident SPPs at the y axis is 1.8 μm. (d) Magnitude of the magnetic field at the metal interface for central position 2.5 μm at the y axis.

4. Conclusion

In this paper, we show several design examples of surface plasmonic devices under the framework of transformation optics and the curved space under coordinate transformations. SPP wave manipulation devices such as a beam squeezer, in-plane bend, and omnidirectional EM absorber are designed and their performances are validated through 3D full-wave EM simulations. Although a rigorous implementation of transformation optics to the SPP manipulations results in the transformation of material on both sides of the dielectric–metal interface, we show that the approximate approach modifying only the dielectric side can lead to a satisfactory performance, therefore it facilitates the realization of the devices. Focusing on practical applications, we also propose simple designs for the SPP wave bend and omnidirectional EM absorber based on the curved space under coordinate transformation. These designs can be realized through conventional dielectric cladding with varying thickness on a metal surface, which can be fabricated by existing nanotechnology, such as gray scale electron beam lithography.[25] All examples demonstrate the significance of transformation optics and the curved space under coordinate transformation for designing a device that manipulates the SPP waves efficiently and flexibly.

References

[1] Pendry J B, Schurig D and Smith D R 2006 *Science* **312** 1780
[2] Leonhardt U 2006 *Science* **312** 1777
[3] Schurig D, Mock J J, Justice B J, Cummer S A, Pendry J B, Starr A F and Smith D R 2006 *Science* **314** 977
[4] Ma H, Qu S B, Xu Z, Zhang J Q and Wang J F 2009 *Chin. Phys. B* **18** 1850
[5] Wang X H, Qu S B, Xia S, Wang B K, Xu Z, Ma H, Wang J F, Gu C, Wu X, Lu L and Zhou H 2010 *Chin. Phys. B* **19** 064101
[6] Rahm M, Schurig D, Roberts D A, Cummer S A, Smith D R and Pendry J B 2008 *Photon. Nanostruct.* **6** 87
[7] Mei Z L and Cui T J 2009 *J. Appl. Phys.* **105** 104913
[8] Kwon D H and Werner D H 2010 *IEEE Antennas Propag. Mag.* **52** 24
[9] Rahm M, Cummer S A, Schurig D, Pendry J B and Smith D R 2008 *Phys. Rev. Lett.* **100** 063903
[10] Xu X, Feng Y and Jiang T 2008 *New J. Phys.* **10** 115027
[11] Tichit P H, Burokur S N and de Lustrac A 2010 *Opt. Express* **18** 767
[12] Narimanova E E and Kildisheva A V 2009 *Appl. Phys. Lett.* **95** 041106
[13] Genov D A, Zhang S and Zhang X 2009 *Nat. Phys.* **5** 687
[14] Cheng Q, Cui J T, Jiang W X and Cai B G 2010 *New J. Phys.* **12** 063006
[15] Chen H Y, Miao R X and Li M 2010 *Opt. Express* **18** 15183
[16] Ebbesen T W, Lezec H J, Ghaemi H F, Thio T and Woff P A 1998 *Nature* **391** 667
[17] Raether H 1988 *Surface Plasmons: on Smooth and Rough Surfaces and on Gratings* (Berlin: Springer) pp. 21–30
[18] Gramotnev D K and Bozhevolnyi S I 2010 *Nat. Photonic.* **4** 83
[19] Barnes W L, Dereux A and Ebbesen T W 2003 *Nature* **424** 824
[20] Kadic M, Guenneau S and Enoch S 2010 *Opt. Express* **18** 12027
[21] Huidobro P A Nesterov M L, Martín-Moreno L and García-Vidal F J 2010 *Nano Lett.* **10** 1985
[22] Liu Y, Zentgraf T, Bartal G and Zhang X 2010 *Nano Lett.* **10** 1991
[23] Huidobro P A Nesterov M L, Martín-Moreno L and García-Vidal F J 2011 *New J. Phys.* **13** 033011
[24] Muamer K, Guillaume D, Chang T M, Guenneau S and Enoch S 2011 *Photon. Nanostruct.* **9** 302
[25] Zentgraf T, Liu Y, Mikkelsen M H, Valentine J and Zhang X 2011 *Nat. Nanotechnol.* **6** 151
[26] Tao J, Huang X G, Lin X S, Zhang Q and Jin X P 2009 *Opt. Express* **17** 13989